Acc. Chem. Res. **1999,** *32,* 145−154

Two-Dimensional Raman Echoes: Femtosecond View of Molecular Structure and Vibrational Coherence

SHAUL MUKAMEL,* ANDREI PIRYATINSKI, AND VLADIMIR CHERNYAK

Department of Chemistry, University of Rochester, P.O. RC Box 270216, Rochester, New York 14627-0216

Received March 6, 1998

I. Introduction

Conventional vibrational spectroscopies such as infrared absorption and spontaneous or coherent Raman scattering provide a one-dimensional projection of intermolecular and intramolecular vibrational structure and motions onto a single frequency (or time) axis. For simple molecules with well-separated eigenstates, this gives direct information on energy levels and their oscillator strengths. The situation is very different in complex systems with highly congested levels such as biological molecules, liquids, polymers, and glasses.[1−5] Here the microscopic information is highly averaged, and is often totally buried under broad, featureless lineshapes, whose precise interpretation remains a mystery. Typical examples are the amide band in proteins,[6,7] and hydrogen-bonded liquids.[8,9]

Shaul Mukamel, Professor of Chemistry at the University of Rochester, NY, and at the Rochester Theory Center for Optical Science and Engineering, received the Ph.D. degree in chemical physics in 1976 from Tel-Aviv University, Israel, and held postdoctoral positions at MIT, Cambridge, and the University of California, Berkeley. His research interests include theoretical studies of ultrafast nonlinear optical spectroscopy in condensed phases, electronic excitations in conjugated and aggregated molecules and semiconductor nanostructures, and biological electron and energy transfer. He is a coauthor of 350 publications and a graduate-level textbook, *Principles of Nonlinear Optical Spectroscopy*, Oxford University Press, 1995. Dr. Mukamel is a fellow of the American Physical Society and of the Optical Society of America, and a recipient of the Fulbright, Alfred P. Sloan, Camille and Henry Dreyfus, Guggenheim, and Alexander von Humboldt Senior Awards.

Andrei Piryatinski received his M.S. degree in theoretical physics in 1992 from Kiev State University, Ukraine, and Ph.D. degree in physics in 1997 from the University of Toledo. Currently he is a postdoctoral fellow at the Chemistry Department of the University of Rochester. His research is focused on theoretical study of luminescence spectroscopy of molecular excitons and ultrafast multidimensional spectroscopy of molecular systems in the condensed phase including liquids and biological molecules.

Vladimir Chernyak received his Ph.D. degree in theoretical and optical physics in 1983 from the Institute of Spectroscopy of the USSR Academy of Sciences. He worked in several research institutions of the USSR National Bureau of Standards and USSR Academy of Sciences. Since 1992 he has been a Senior Scientist at the Chemistry Department of the University of Rochester. His research interests include theoretical studies of ultrafast dynamics in molecular aggregates, semiconductor nanostructures, and biological complexes, optical properties of disordered systems, and electronic excitations in large organic molecules.

For decades, optical spectroscopists have dreamt about using multidimensional coherent nonlinear spectroscopic techniques to overcome these difficulties and unravel the microscopic picture underlining complex spectra. Coherent spectroscopy uses several laser beams to generate signals that propagate along new directions, different from those of the incoming pulses. "Coherent" implies that phase information plays an important role. In this context, coherence has a dual meaning corresponding to both the radiation field and the molecules. First, the signal field is generated by many molecules whose externally driven charge distributions oscillate in phase, creating a signal field with a well-defined phase. This is in contrast to incoherent techniques such as fluorescence where individual molecules contribute additively to the signal's *intensity* rather than to the *amplitude*, and there is no phase relation between the light emitted by different molecules. In addition to the phase of the field, the laser beams create wavepackets of molecular states; coherence thus further implies a definite phase relationship between different states. Multiple pulses can create, manipulate, and probe this coherence which carries important signatures of molecular structure, coupling patterns, and dynamics.

Many modern techniques in spectroscopy make use of coherence. For example, one of the major accomplishments of nuclear magnetic resonance has been its capacity to disentangle hopelessly complicated spectra by spreading them in more dimensions onto several frequency or time axes.[10] Carefully designed pulse sequences make it possible to eliminate dipolar interactions which dominate the line widths. Since their inception in the 1970s, multidimensional NMR techniques have turned into a powerful tool which provides structures with resolution comparable to X-rays, and dynamics of very complex molecules, crystals, and proteins with up to a few thousand atoms. Multidimensional spectroscopy probes correlations between signals and offers an unusual sensitivity and selectivity. Magnetic resonance is the elder brother of coherent optical spectroscopy: the two share many basic concepts. Since the ability to shape and control radiowave pulses predated similar advances in laser technology, many of the optical techniques had been invented in NMR 20−30 years earlier. By extending these ideas to the optical regime, it should be possible to come up with novel classes of spectroscopies which could probe complex vibrational motions. Picosecond coherent spectroscopy of atoms and small molecules in the gas phase is very similar to that of nuclear spins.[11,12] The extension to complex molecules in the condensed phase has been a much more difficult task which requires some significant advances. The large transition dipoles and strong interactions induce line broadenings resulting from ultrashort dephasing processes, which the excitation pulses need to overcome. The necessary impulsive excitation requires laser pulses shorter than the corresponding vibrational periods and dephasing timescales. In recent years, femtosecond laser techniques have made giant strides, and

10.1021/ar960206y CCC: $18.00
Published on Web 11/06/1998

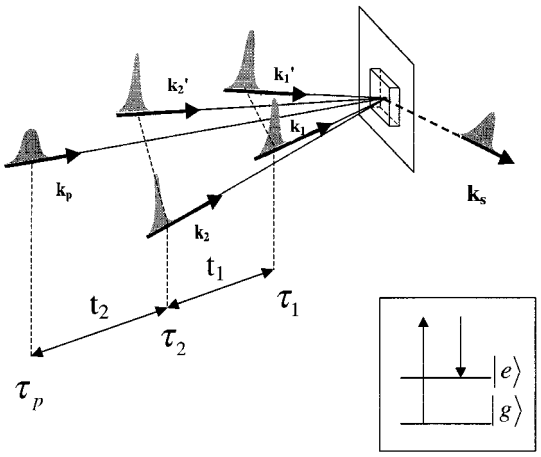

FIGURE 1. Geometry and time-ordering of the incoming pulse sequence in a fifth-order 2D spectroscopy. $\Delta\mathbf{k}_1 \equiv \mathbf{k}_1 - \mathbf{k}'_1$, $\Delta\mathbf{k}_2 \equiv \mathbf{k}_2 - \mathbf{k}'_2$.. Only one of the nine possible signal pulses in the direction $\mathbf{k}_s = \Delta\mathbf{k}_1 + \mathbf{k}_p$ is shown. Inset shows the elementary Raman process. A pair of impulsive pulses E_j interacts twice with the molecule, initially in state $|g\rangle$, to create a coherent superposition of vibrational states $|g\rangle$ and $|e\rangle$. ($|g\rangle\langle e|$). The amplitude of this process is αE_j^2. The probe works in reverse: the $|g\rangle\langle e|$ coherence is converted into a population $|g\rangle\langle g|$ or $|e\rangle\langle e|$ with an amplitude αE_p (one of the transitions is now spontaneous, hence the linear dependence on the field).

the complete control of the optical electric field (pulse shapes, durations, and even phases) is now possible.[13] The theoretical challenge is very demanding as well: spins are elementary quantum systems whose Hamiltonians depend on a few universal parameters. Anharmonic vibrations are much more difficult to model: the mere task of writing the vibrational Hamiltonian requires as extensive electronic structure calculation of a potential surface. Other fundamental differences between multidimensional NMR and optical techniques will be outlined as we go along.

Probing molecular vibrations with visible pulses requires a Raman process (inset in Figure 1) whereby two interactions with light prepare a superposition of two (or more) vibrational states with a well-defined phase (vibrational coherence). Multidimensional spectroscopy involves the application of n pairs of well-separated pulses which generate vibrational coherence in the ground electronic state, followed by a final probe pulse which is scattered off the sample.[14] We assume that all pulse pairs (j, j'), centered at τ_j, have identical envelopes $E_j(\tau - \tau_j)$ but different wavevectors ($\mathbf{k}_j$, $\mathbf{k}_{j'}$). The probe envelope is $E_p(\tau - \tau_j)$ and direction $\mathbf{k}_p$ (Figure 1). (The wavevector is a vector pointing in the direction of propagation and whose magnitude is 2π divided by the wavelength of the light). If the optical fields are tuned off-resonant with respect to all electronic transitions, the coupling of the vibrational degrees of freedom to the driving field $E(\tau)$ can be described by the effective interaction $-\alpha(\mathbf{Q})E^2(\tau)$, where $\alpha(\mathbf{Q})$ is the electronic polarizability whose dependence on the nuclear configuration $\mathbf{Q}$ provides the window for observing vibrational motion.[15]

The signal field is calculated by summing the contributions of all molecules in the sample. The sample size is typically much larger than the optical wavelength, and consequently the various contributions have different phases, and when added up, the sum will vanish in almost all directions. There are however a few special directions whereby the fields add in phase, resulting in a coherent signal. These *phase-matching* directions correspond to all possible wavevectors obtained by a superposition of the incoming ones, i.e., $\mathbf{k}_s = \pm\Delta\mathbf{k}_1 \pm \Delta\mathbf{k}_2 \ldots \pm \Delta\mathbf{k}_n + \mathbf{k}_p$, where $\Delta\mathbf{k}_j \equiv \mathbf{k}_j - \mathbf{k}'_j$. Altogether the signal field is $(2n+1)$th order in the applied fields. Since n time intervals between pulses are independently controlled, this technique constitutes an n-dimensional (nD) spectroscopy.

The electronically off-resonant coherent Raman scattering (CRS) which is the lowest (1D, third-order) technique of this type has long been used for probing vibrational frequencies, relaxation, and dephasing rates.[16,17] Loring and Mukamel have pointed out that due to its one-dimensional nature, this technique carries precisely the same information as ordinary light scattering (spontaneous Raman spectroscopy). In fact, the two are related by a simple Fourier transform.[14] They have further shown that multidimensional techniques in which independent control over several time intervals between short pulses is maintained should provide a much more sensitive probe for the structure and dynamics of molecules in the condensed phase. The first suggestion was to conduct the Raman analogue of the photon echo, which is a seventh-order (3D) technique.[12,14,18] Several experiments have subsequently been carried out in order to measure the homogeneous vibrational linewidth of high-frequency intramolecular vibrations in molecular liquids.[12,19,20] Tanimura and Mukamel have later showed how lower (fifth-order, 2D) techniques may be effectively used to probe the nature of molecular vibrations.[21] The fifth-order echo probes correlations between different transitions, which the standard echo does not. This unexpected predicition had triggered extensive experimental[22,23] and theoretical[22,24,25] activity focused on the application of this technique to probe intermolecular nuclear dynamics in liquids.

In this Account we review the theoretical and experimental progress made in this new and rapidly developing field. Our analysis will focus on the fifth-order Raman techniques; however, the main ideas can be applied to higher order processes as well, and to the closely related infrared measurements.[3,26] The field is still at its infancy, and considerable experimental and theoretical effort will be required in order to develop it into a routine structural and dynamical tool.

II. One-Dimensional (Third-Order) Response of a Multimode Harmonic System

CRS uses three pulses to generate the signal at $\mathbf{k}_s = \mathbf{k}_1 - \mathbf{k}'_1 + \mathbf{k}_p$. This 1D signal is described by the two-time correlation function of the electronic polarizability $\langle\alpha(\tau_1)\alpha(\tau_2)\rangle$. Here the time evolution of the polarization $\alpha(\tau)$ is given by the pure molecular Hamiltonian (in the

absence of the driving field). The correlation function represents equilibrium fluctuations of α, and only depends on the time difference $\tau_1 - \tau_2$. It can be easily evaluated using the complete set of vibrational eigenstates of the system $g, e, f, \ldots$ with energies $\epsilon_g, \epsilon_e, \epsilon_f, \ldots$. The signal field amplitude is then given by

$$S^{(3)}(t_1) = \sum_{g,e} P(g)|\alpha_{ge}|^2 \sin[\Omega_{eg}(t_1)] \qquad (2.1)$$

where t_1 is the delay between pulses, $P(g)$ is the equilibrium population of state g and $\hbar\Omega_{eg} = \epsilon_e - \epsilon_g$. This apparently simple expression may only be used for small systems with sparse, well-resolved levels. In such systems 1D spectroscopies provide the complete information, and 2D techniques are superfluous. However, it is impractical to describe the dynamics of complex systems in the condensed phase using their global eigenstates. These states are very hard to calculate and carry much more information than provided by spectroscopic measurements: a description in terms of the global states is neither feasible nor desirable, and different (e.g., semiclassical) descriptions may become more useful.

Earlier applications of CRS focused on isolated vibrational lines corresponding to high-frequency intramolecular vibrations.[16,17] We shall discuss this case first. Theoretical modeling can then be done by separating the vibrational modes into a few Raman active modes coupled to continuous distributions of low-frequency bath modes whose effect is incorporated through line broadening (dephasing) of the Raman modes. Spectral lineshapes are traditionally classified as either homogeneous (when the underlying bath motions are very fast compared to the inverse linewidths) or inhomogeneous (when these motions are slow). In the following we assume a single harmonic primary mode coupled linearly to the radiation field (i.e., α is proportional to the coordinate) and to the surroundings. We further assume a Lorentzian homogeneous broadening with width γ, and represent the static disorder of local environments by a Gaussian inhomogeneous distribution of the frequency Ω with the mean Ω_0 and variance Δ.

Depending on the laser field used, the molecular information can be retrieved either in the time domain or in the frequency domain. Three types of techniques may be identified. (i) *Impulsive.* For pulses short compared with all other timescales (i.e., the vibrational periods Ω_0^{-1}, and dephasing times γ^{-1}, Δ^{-1}),[27] the time-resolved signal shows coherent vibrations as well as their dephasing.

$$S_i^{(3)}(t_1) \sim \sin(\Omega_0 t_1) \exp\left(-\gamma t_1 - \frac{\Delta^2 t_1^2}{2}\right) \qquad (2.2)$$

All molecular parameters are now obtained in the time domain. (ii) *Semi-impulsive.* In this intermediate case the pulses are short compared with γ^{-1} and Δ^{-1} but long compared with Ω_0^{-1}. These techniques lack the time resolution to observe vibrational motions directly. The signal assumes the form of eq 2.2 but without the $\sin(\Omega_0 t)$ term, and its decay with the delay between the excitation and the probe pulses only reflects vibrational dephasing. The dephasing rates γ and Δ are thus obtained in the time domain whereas the frequency Ω_0 is obtained in the frequency domain by tuning the pulses and selecting the mode to be observed. (iii) *Continuous wave* (cw). When the pulses are long compared with Ω_0^{-1}, γ^{-1}, and Δ^{-1}, the signal is given by the Fourier transform of of eq 2.2. For our model this gives a Voigt profile (a convolution of a Gaussian and a Lorentzian) showing Raman resonances when $\omega_1 - \omega_2 = \Omega_0$. Ω_0, γ, and Δ are now obtained in the frequency domain, by scanning $\omega_1 - \omega_2$. Femtosecond, picosecond, and nanosecond techniques typically correspond to these three regimes, respectively. Spontaneous Raman signals are closely related to their cw coherent Raman counterparts. The corresponding expressions only differ by some prefactors.[27]

Since 1D measurements provide a highly averaged picture of nuclear structure and dynamics, different microscopic models may be consistent with a given 1D signal. For example, if we observe several vibrational lines, it is impossible to tell whether they represent coupled or decoupled transitions, or what type of coupling is involved (purely electrostatic dipole−dipole type coupling of localized vibrations or when both vibrations are coupled to the same electronic state). Moreover, since both homogeneous and inhomogeneous relaxations enter $S_i^{(3)}$ in an identical fashion (a product in the time domain or a convolution in the frequency domain), it is impossible to tell them apart. If we have some prior knowledge about these lineshapes, e.g., if we know that the homogeneous contribution is Lorentzian whereas the inhomogeneous profile is Gaussian, and if the corresponding linewidths are not very different, it may be possible to deconvolute the 1D signal into these separate contributions. However, this procedure is model-dependent and does not constitute a genuine separation based on the bath timescale.

Early picosecond coherent Raman measurements were incorrectly believed to have the capacity of selectively eliminating inhomogeneous vibrational dephasing and revealing the homogeneous component. Only when the process was formulated in terms of correlation functions it became evident that this electronically off-resonant 1D Raman technique is nonselective in principle, and that higher-order multidimensional techniques such as the Raman echo are required to probe selectively the homogeneous linewidth.[14]

In addition to high-frequency vibrations, femtosecond CRS measurements have been used to study the lower-frequency intermolecular motions in liquids.[28] The time evolution is in this case much more complex, and the Fourier transform of the signal gives continuous spectral densities which provide characteristic signatures of intermolecular nuclear degrees of freedom, both local and collective. The applicability of quasiharmonic models to intramolecular vibrations is well established. However, this is not necessarily the case for intermolecular motions. An instantaneous normal mode procedure has been proposed for the description of intermolecular modes in liquids.[29] Generally collective modes may have Gaussian

statistics due to the central limit theorem, and may be considered harmonic even though the underlying microscopic motions may be far from that. A typical example is the 1D Raman spectrum of liquid water shown in Figure 5A. It is impossible to tell, on the basis of this spectrum alone, whether the underlying vibrational motions are fast (homogeneous spectral density) or slow (inhomogeneous). Moreover, vibrational motions in complex systems typically span a broad range of timescales, reflecting their complicated many-body interactions. In proteins, for example, these range from femtosecond motions of individual vibrations[3] all the way to protein folding (seconds).[7,30] Under these conditions vibrational lineshapes and spectral densities cannot be simply classified as either homogeneous or inhomogeneous. The interpretation of multidimensional spectroscopies using correlation functions does not rely on this classification, but allows us to use it when applicable.

III. Two-Dimensional (Fifth-Order) Response

The 2D response is obtained when the system is subjected to two pairs of excitation pulses followed by the probe.[21] The corresponding signal field $S^{(5)}(t_2,t_1)$ is related to the three-point correlation functions $\langle\alpha(\tau_3)\alpha(\tau_2)\alpha(\tau_1)\rangle$. We illustrate the 2D response using a microscopic model. The simplest model that comes to mind assumes harmonic vibrations with linear dependence of α on nuclear displacements. However, this model, used in section II, is strictly linear since the induced signal field is always proportional to the driving field $E^2(\tau)$. The only finite response is then $S^{(3)}$, and all higher signals $S^{(5)}$, $S^{(7)}$, etc. vanish identically. To see that, we note that the signal is given by a sum of four contributions, each represented by the three-point correlation function with a different choice of time arguments. Each of these contributions represents a distinct Liouville space pathway for the system's density matrix.[27] (More generally $S^{(2n+1)}$ will have 2^n pathways.) A Liouville space pathway provides a formal representation of system dynamics in terms of possible sequences of populations and superposition states. When all the terms are carefully added, they cancel, reflecting a destructive interference of various nonlinear paths. Optical response higher than $S^{(3)}$ can be induced by adding various sources of nonlinearity which remove this exact cancellation. Possible sources are (i) nonlinear dependence of α on nuclear coordinates $\alpha \sim \alpha^{(N)}_{j_1\ldots j_N} Q_{j_1}\ldots Q_{j_N}$, (ii) anharmonic potentials which contain terms cubic and higher in the coordinates $V(\mathbf{Q}) \sim V^{(N)}_{j_1\ldots j_N} Q_{j_1}\ldots Q_{j_N}$, and (iii) relaxation by nonlinear coupling to a bath. The 2D optical response can be represented as a superposition of elementary processes each involving up to three eigenstates of the system denoted as $|g\rangle$, $|e\rangle$, and $|f\rangle$ with energies ϵ_g, ϵ_e, and ϵ_f, respectively (see Figure 3). The signal can be interpreted in terms of statistical properties of the system's eigenstates, expressed using two-dimensional spectral densities.[31]

Multidimensional techniques provide a wealth of information. Coherence transfer which takes place along the Liouville space paths depends critically on molecular structure and mode couplings. New peaks, their intensities, and profiles constitute a sensitive probe of molecular structure and dynamics. These will be illustrated next.

A. Information Contained in Line Positions: Cross Peaks. If the various vibrational modes do not interact, the nonlinearities will be diagonal $\alpha^{(2)}_{jj}$, $V^{(3)}_{jjj}$, and the contributions of the various modes to the nonlinear response will be additive. Off-diagonal couplings $\alpha^{(2)}_{jk}$, $V^{(3)}_{jkl}$ will however result in cross terms. Different models may give the same $S^{(3)}$ but a very different $S^{(5)}$. The 2D signal can be displayed in the frequency domain by defining the Fourier transform of $S^{(5)}(t_2,t_1)$ with respect to t_1 and t_2.[3,32] It should be emphasized that the resulting $S^{(5)}(\omega_2,\omega_1)$, despite its frequency domain appearance, represents a time domain technique (which is merely displayed in ω-space) since it maintains a complete control over time-ordering; ω_1 is associated with the first time interval and ω_2 with the second. ω_1 and ω_2 thus carry different types of information. This is in contrast with genuine frequency domain measurements described by optical susceptibilities which are invariant to permutations of field frequencies.[27]

2D Raman spectroscopy of coupled localized high-frequency vibrations can best be described using an exciton model.[26,33] The nonlinear exciton equations (NEE) developed for the treatment of electronic excitations in chromophore aggregates provide a closed algorithm for computing the optical response.[27,31] In the following we display the signals calculated perturbatively in the nonlinearities. In Figure 2 we present a contour plot of $|S^{(5)}(\omega_2,\omega_1)|^2$ calculated for a model system of two coupled harmonic vibrations with frequencies $\Omega_a = 170\ \mathrm{cm}^{-1}$ and $\Omega_b = 260\ \mathrm{cm}^{-1}$. The signal is proportional to $\alpha^{(2)}_{nm}\,\alpha^{(1)}_{n}\,\alpha^{(1)}_{m}$. The decoupled mode case (i.e., α_{nm} is diagonal) is shown in panel A. This plot consists of (ω_1,ω_2)-resonances on the oscillator frequencies $(\pm\Omega_n,\ \pm\Omega_n)$, $n = a,\ b$ (unmarked), as well as overtones $(\Omega_n, 2\Omega_n)$, $(-\Omega_n, -2\Omega_n)$, and zero-frequency resonances $(\pm\Omega_n, 0)$. When both diagonal and off-diagonal components of $\alpha^{(2)}_{nm}$ are included, we obtain the signal shown in panel B. In addition to the peaks of panel A, intermode coupling (via off-diagonal $\alpha^{(2)}_{nm}$ terms) induces ω_2-resonances on combination of frequencies (*cross-peaks*) such as $(\Omega_b,\ \Omega_a + \Omega_b)$. Adding a $V^{(3)}_{nml}$ anharmonicity does not change the nature of the pattern. The same peaks show up; however, their relative intensities are affected. The two types of nonlinearity enter the response in a different way: The polarizability ($\alpha^{(2)}_{nm}$) creates intermode coherences instantaneously, each time the system interacts with the radiation field. In contrast, the effect of anharmonicity ($V^{(3)}_{mnk}$) is not felt immediately since such a coherence may only be built during the evolution period between interactions (see the phase shift in eq 3.1). The connection between anharmonicities and nonlinearities allows us to gradually look deeper into anharmonicities by using high-order techniques. Higher order techniques examine larger amplitude motions where anharmonic effects are more pronounced.

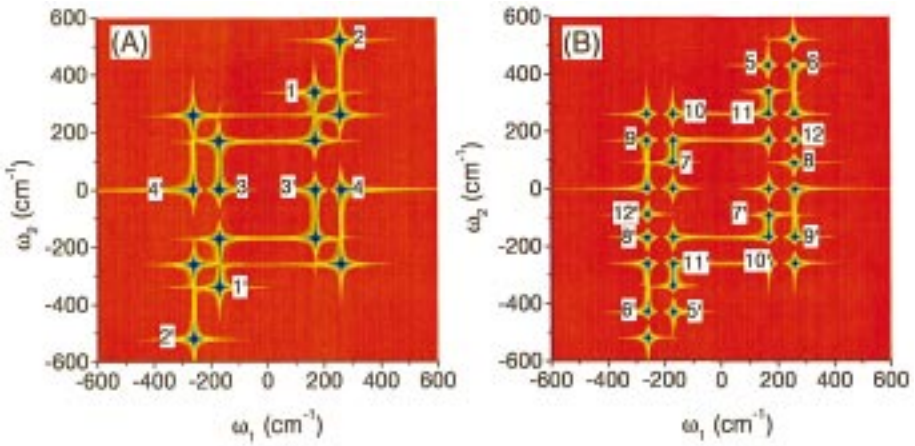

FIGURE 2. 2D Raman spectrum of two harmonic vibrations ($\Omega_a = 170$ cm^{-1} and $\Omega_b = 260$ cm^{-1}). (A) Second-order polarization nonlinearity is diagonal ($\alpha^{(2)}_{11} = \alpha^{(2)}_{22} = 1$, $\alpha^{(2)}_{12} = \alpha^{(2)}_{21} = 0$). The modes are decoupled and resonances show oscillator frequencies (unmarked) as well as overtones (1) (Ω_a, $2\Omega_a$), (2) (Ω_b, $2\Omega_b$) and zero-frequency resonances (3) ($-\Omega_a$, 0), (4) (Ω_b, 0). The overtones 1′−2′ and zero-frequency peaks 3′−4′ are obtained by inversion symmetry of 1−4 peaks. (B) All components of the polarization nonlinearity are included ($\alpha^{(2)}_{11} = \alpha^{(2)}_{22} = \alpha^{(2)}_{12} = \alpha^{(2)}_{21} = 1$); cross-peaks (5) ($\Omega_a$, $\Omega_a + \Omega_b$), (6) (Ω_b, $\Omega_a + \Omega_b$), (7) ($-\Omega_a$, $\Omega_b - \Omega_a$), (8) (Ω_b, $\Omega_b - \Omega_a$) and resonances such as (9) ($-\Omega_b$, Ω_a), (10) ($-\Omega_a$, Ω_b), (11) (Ω_a, Ω_b), (12) (Ω_b, Ω_a) are due to the intermode coupling via the off-diagonal elements and $\alpha^{(2)}_{21}$. Peaks 5′−12′ are related to 5−12 by inversion symmetry.

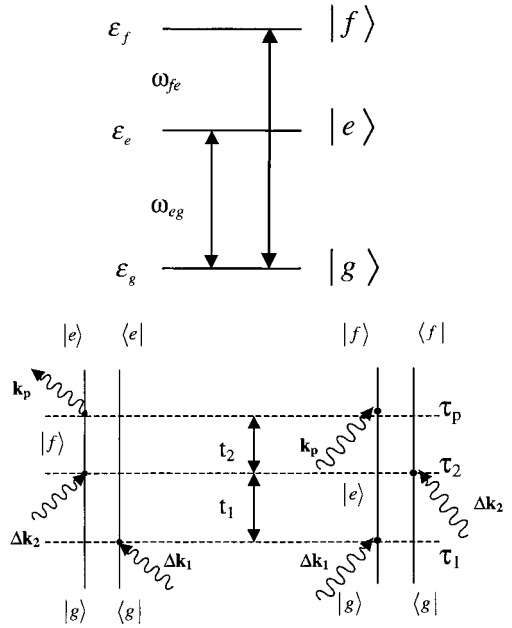

FIGURE 3. Vibrational level scheme and the Feynman diagrams representing the Liouville space pathways (sequence of coherences) excited by the (2D) five-pulse sequence. Before the excitation, the density matrix is in the state $|g\rangle\langle g|$; during t_1 and t_2 it is in the coherent superposition states $|e\rangle\langle g|$ and $|e\rangle\langle f|$, respectively. The 2D signal can be traced back to two-dimensional spectral density $\kappa(\epsilon', \epsilon'')$ defined as the sum of contributions to the response from all elementary processes with $\epsilon_e - \epsilon_g = \epsilon'$, $\epsilon_f - \epsilon_e = \epsilon''$. Inhomogeneous and homogeneous dephasing rates control the width of the distribution of $\epsilon' + \epsilon''$ and $\epsilon' - \epsilon''$, respectively. An echo is generated when the fluctuations in transition energies ϵ' and ϵ'' are strongly correlated so that the distribution of $\epsilon' - \epsilon''$ is narrow.[32]

Cross-peaks provide a direct probe for intermode couplings. Useful structural information can thus be derived from the intensities of cross-peaks between localized vibrations (either on the same molecule or on different molecules). For example, cross-terms in α may arise either when two vibrations couple to the same electronic state or due to excitonic electrostatic coupling (local field effects) that involves no electron delocalization. Multidimensional techniques should be able to distinguish between the two mechanisms through the variation of peak intensities with detunings of the pulses. A word of caution: The observed signal depends on the detection mode.[27] Ordinary homodyne detection probes $|S^{(2n+1)}|^2$. However, heterodyne phase-controlled techniques can probe the signal field $S^{(2n+1)}$ itself (both amplitude and phase). Cross-terms appear in the homodyne signal even when they are absent in $S^{(2n+1)}$ itself. This is a macroscopic effect (generated by interference between electric fields) and yields no additional microscopic information, even though it may provide a convenient detection mode.[34] Multidimensional Raman spectroscopy constitutes an ideal tool for probing complex protein structure. For example, cross-peak patterns of localized CO vibrations of the amide band should provide a sensitive probe for its secondary and tertiary structure, as suggested by infrared studies.[6,26,33]

B. Looking into the Lineshapes: Photon Echoes. We now consider a single intramolecular high-frequency mode and focus on the role of homogeneous and inhomogeneous broadening induced by its coupling to a bath. The impulsive signal, averaged over the inhomogeneous distribution, contains the following contribution:

$$S_i^{(5)}(t_2, t_1) \sim \exp[-\gamma(t_1 + t_2)] \exp\left[-\frac{\Delta^2(t_2 - t_1)^2}{2}\right] \times \cos[\Omega_0(t_2 - t_1) + \theta] \quad (3.1)$$

where the phase shift θ depends on the relative values of anharmonicity ($V^{(3)}$) and nonlinearity ($\alpha^{(2)}$) contributions to the optical response.

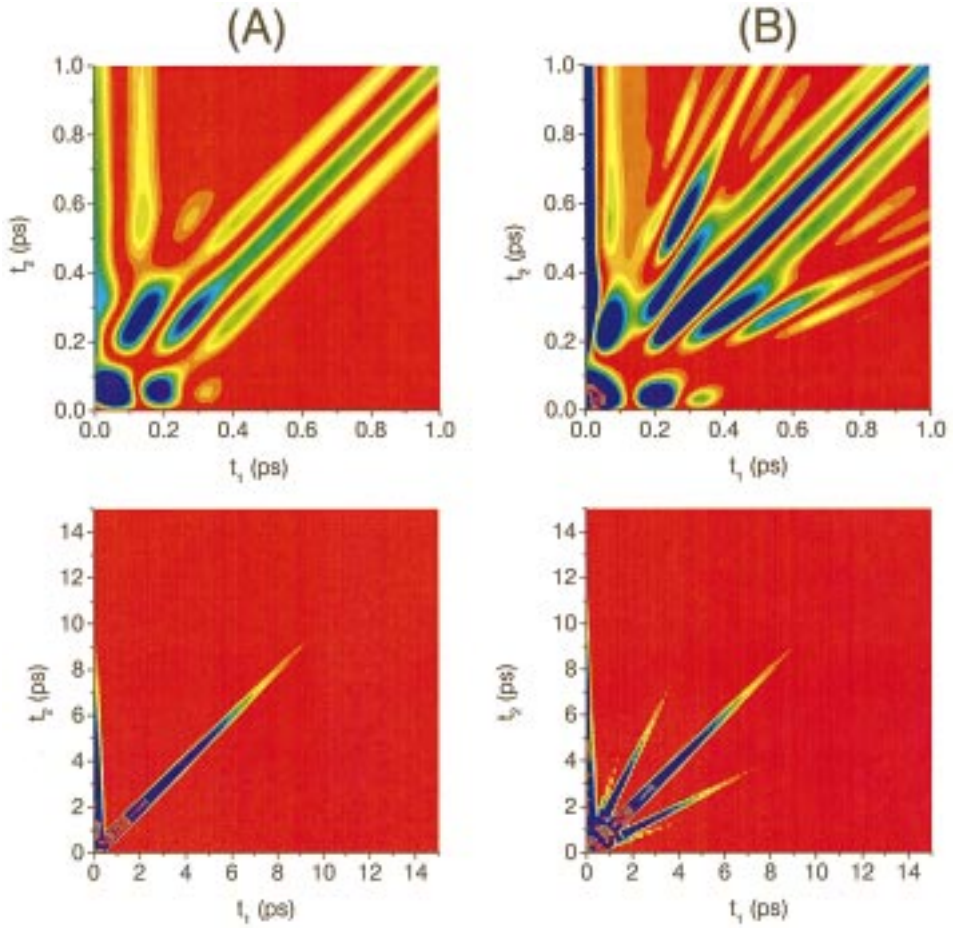

FIGURE 4. Contour plots of the 2D signal $|S(t_1, t_2)|^2$ for a harmonic model in high-temperature limit (i.e., $kT \gg \hbar\Omega_0$) with exponential nonlinearity, averaged over Gaussian frequency distribution ($\Omega_0 = 112$ cm^{-1}, $\Delta = 30$ cm^{-1}, and $\gamma = 1$ cm^{-1}) for different values of the dimensionless nonlinearity $g_T = (2kT)/(M\Omega_0^2 Q_0^2)$. Upper panels, short time (expanded scale). Lower panels, long time. (A) $g_T = 1 \times 10^{-4}$. The only echo appears in the direction $t_1 = t_2$. (B) $g_T = 0.5$. Additional echoes originating from coherences between higher levels are well resolved for $t_1 = 2t_2$ and $t_2 = 2t_1$. In all plots the signal along t_2 for $t_1 = 0$ is associated with vibrational population.

We shall assume that inhomogeneous broadening is dominant ($\Delta \gg \gamma$). Let us set $t_2 = 0$ and consider long times t_1 compared with the inhomogeneous decay timescale $T_I \equiv \Delta^{-1}$, where the signal has vanished (apparently irreversibly). As t_2 is increased, we note a remarkable effect: at $t_2 = t_1$, the contribution of Δ is cancelled and the signal shows up again as an "echo". Observing the signal vs t_1 gives information about Ω_0 and γ that is not available from $S^{(3)}$ when $\Delta \gg \gamma$. Anharmonicities in general introduce additional frequencies which will show up as oscillations (quantum beats) in the optical response.[3] If the anharmonicities are sufficiently weak, these low-frequency beats are not observed and their only effect is to introduce a phase shift.

In the above example only the lowest two vibrational states participate in the response. As the nonlinearity is increased, more levels enter into the picture and one can observe multiple echoes in various directions. To illustrate this, let us consider a single primary harmonic vibration with frequency Ω_0 and homogeneous dephasing γ where $\gamma \ll \Omega_0$ (this is an underdamped Brownian oscillator). Its electronic polarizability depends exponentially on the coordinate $\alpha(Q) = \alpha_0 \exp(Q/Q_0)$.[27] $|S^{(5)}(t_1, t_2)|^2$ is shown in Figure 4. Columns A and B display the signal calculated for different values of the nonlinearity parameter $1/Q_0$. Multiple echoes can show up in all directions $t_2 = nt_1/m$, where m and n are integers. These represent different sequences of multiquantum coherences between successively higher levels: $|j\rangle\langle j + n|$ during the t_1 time interval, followed by $|j + m + n\rangle\langle j + n|$ during t_2. For weak nonlinearity, the only echo corresponds to $m = n = 1$ and occurs at $t_2 = t_1$ (Figure 4A), independent of the frequency Ω_0. The echo decay reflects the homogeneous dephasing timescale $T_2 = \gamma^{-1}$. Multiple echoes are clearly seen in panel B, where the nonlinearity is increased. The width of the mth echo along the t_2 direction (T_I/m) is independent of n. The lower panels show that the echo decays with the dephasing timescale γ^{-1}. Oscillations with frequency $m\Omega_0$ can be seen in the upper panels, which is plotted on an expanded timescale. As long as $\Delta \ll \Omega_0$ the various echoes are well-resolved since the signals have different frequencies Ω_m. For $\Delta \approx \Omega_0$ the echoes may not be resolved. In the frequency domain the signals merge, and interference between higher-order signals may destroy the echo.

In addition, the 2D plots contain a signal stretched along the t_2 axis which corresponds to $m = 0$ and originates from the evolution of vibrational population

$|j + n\rangle\langle j + n|$ during the second time interval t_2. 1D spectroscopy cannot distinguish between vibrational relaxation (T_1) and homogeneous ($T_2 \equiv \gamma^{-1}$) and inhomogeneous ($T_I \equiv \Delta^{-1}$) dephasing times. However, in 2D spectroscopy they can be clearly separated: The signal along the echo direction decays with timescale T_2. The $m = 0$ signal stretched along the t_2 axis with $t_1 = 0$ will decay on the T_1 timescale. In all other (nonecho) directions the signal will decay with the T_I timescale. *A single 2D measurement clearly provides all three of these important timescales!*[35]

Intermolecular vibrations are by far more complex than intramolecular, low-frequency modes. 1D measurements usually result in continuous spectral densities containing a few broad peaks and extending over hundreds of wavenumbers, which are very hard to interpret. The experimental 1D spectral density of liquid water which can be fitted to a six Brownian oscillator model is shown in Figure 5A. In addition the figure shows the calculated 2D signals obtained by assuming that the 1D spectral density is either homogeneous (B) or inhomogeneous (C).[36] An echo signal peaked at $t_1 = t_2$ is seen only in the inhomogeneous case. This illustrates the additional information carried by 2D signals: Many possible microscopic models have the same 1D spectra but very different 2D response. Experimental studies of the fifth-order nonlinear response in liquids have been reported in refs 20−23 2D studies of CS_2 show a nonecho type of response (like Figure 5B). The asymmetry of the signal along the t_1 and t_2 axes cannot be reproduced by simple models such as the one described earlier with $\alpha^{(2)}$ and $V^{(3)}$. A higher level modeling of these measurements is required. Suppression of the photon echo due to the vibrational mode coupling via $\alpha^{(2)}$ in liquid water and liquid CS_2 has been demonstrated by numerical simulations.[25] An important challenge is the identification of collective coordinates which should allow a microscopic description of the relevant intermolecular motions.

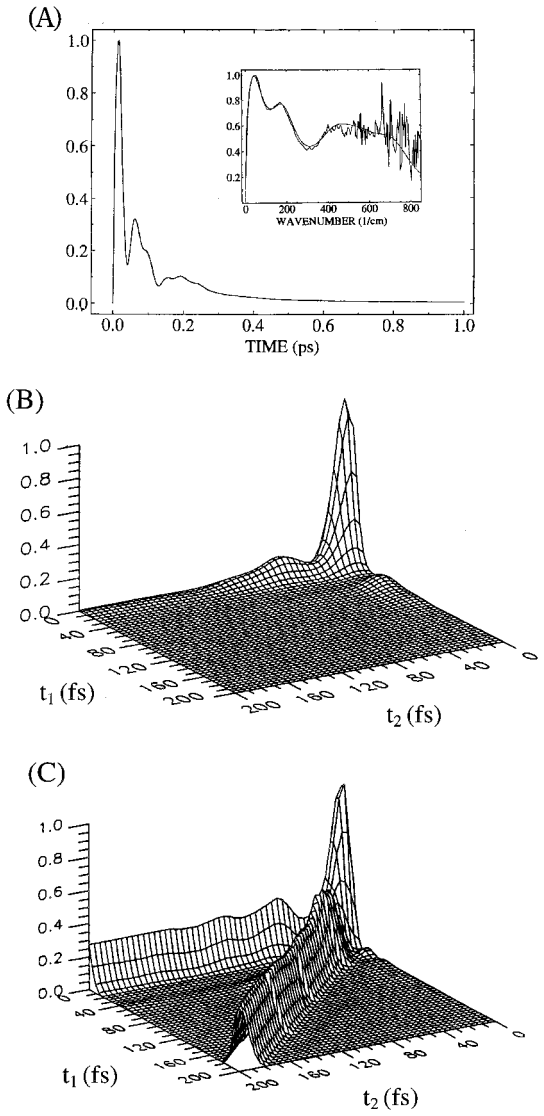

FIGURE 5. (A) Impulsive Raman signal and its Fourier transform. The spectral density (inset) measured by 1D spectroscopy of liquid water can be well represented as a superposition of six Brownian oscillators (solid lines in both plots).[36] The following two panels display the fifth-order response calculated by assuming that the 1D spectral density (A) is either homogeneous (panel B) or inhomogeneous (panel C). An echo peaked at $t_1 = t_2$ is clearly seen in (C).

IV. Design of New Pulse Sequences and Comparison with NMR

The multidimensional signal $S^{(2n+1)}$ is computed by convoluting a multidimensional response function with the incoming pulse envelopes.[27] An optical pulse can be generally represented in the form[13]

$$E_j(\tau) = E_j(\tau + t_j)\exp[-i\bar{\omega}_j\tau + i\varphi_j] + cc \qquad (4.1)$$

Pulse-shaping techniques make it possible to vary the envelopes $E_j(\tau)$ and time delays t_j, tune the frequencies $\bar{\omega}_j$, and vary the phases φ_j. By scanning these various parameters, it is possible to custom design a multiple pulse technique for a specific system and purpose. So far we focused our attention primarily on the conceptually simplest, heterodyne techniques carried out with impulsive pulses where pulse durations are much shorter than both the delay between pulses and the nuclear dynamics timescales. The time-resolved signal field is then proportional to the response function itself. In this limit the only relevant information about the pulses is their time intervals. Additional information about pulse frequencies enters when longer, semi-impulsive, pulses are employed (as defined in section II). Two important differences with the impulsive signal (eq 3.1) are then observed. First, the semi-impulsive signal does not resolve the frequency Ω_0 since the pulses cannot excite vibrations coherently. Second, semi-impulsive signals depend on the pulse central frequencies as well, carry a different phase, and have a different time profile in various directions. Finite pulses can select specific Liouville space pathways which are resonant for a given pulse configuration and carry a well-defined combination of $\Delta\boldsymbol{k}_j$ factors. An echo is then generated only in one specific direction, $\boldsymbol{k}_s = \boldsymbol{k}_p + \Delta\boldsymbol{k}_2 - \Delta\boldsymbol{k}_1$. In contrast, the impulsive signal has no spatial selectivity: the same impulsive signal is generated in all

nine possible directions of $S^{(5)}$, $\mathbf{k}_s = \mathbf{k}_p + m\Delta\mathbf{k}_1 + n\Delta\mathbf{k}_2$, $n, m = 0, \pm 1$.

Further advances in theoretical modeling will be required in order to develop these techniques into standard diagnostic tools. Methods for classical and quantum simulations of two-point correlation functions are well established.[8,37] The development of efficient sampling algorithms and simulation strategies for computing multiple time correlation functions poses an interesting open challenge. This is crucial for the interpretation of multidimensional techniques using realistic microscopic models. Special attention needs to be paid to interference effects between closely lying trajectories which are absent in $S^{(3)}$ but are essential for all higher order responses such as $S^{(5)}$.[38] The information content of various experimental configurations should be systematically classified and compared. Theoretical models and algorithms for inverting experimental data to extract the desired structural and dynamical information need to be constructed. Multiple pulse NMR techniques are so well developed that nonmathematical diagrammatic sketches can be effectively employed by nonspecialists toward their design and interpretation. Similar simple qualitative pictures for multidimensional Raman spectroscopies are yet to be developed.

Short pulses can create wavepackets (i.e., superpositions of states with well-defined phases and amplitudes). In simple systems with a few degrees of freedom, quantum beats observed in different measurements (pump−probe, fluorescence, photon echo) provide direct signatures for the evolution of these coherent wavepackets.[27] The observation of such wavepackets in complex systems with a macroscopic number of degrees of freedom seems unlikely at first glance, since fast dephasing is expected to very rapidly destroy all coherences. Nevertheless, carefully designed nonlinear measurements may probe vibrational coherence. This state of affairs is completely analogous to magnetic resonance:[10] the creation of coherence in a single spin is straightforward. However, coherent spectroscopy of many interacting spins has only been made possible by ingenious multiple pulse techniques.

Despite the striking conceptual similarity, multidimensional Raman techniques differ from their NMR counterparts in several important ways. In resonant NMR techniques, the solvents are transparent and the signal is generated by the species of interest. In off-resonant techniques such as Raman, contributions from the solvent are substantial and need to be carefully eliminated. In NMR the high-temperature limit usually applies (kT is much larger than transition frequencies). This means that the one-dimensional (single-quantum) spectra are very complex, and they become simpler for multiquantum transitions (since there are fewer of them). High-frequency vibrations are closer to the opposite, zero temperature, limit: Here the single-quantum spectrum is simple and multiquantum spectra are more complex.

NMR measurements are usually semi-impulsive (although weak-field NMR and nuclear quadropole resonance NQR used in medical imaging are sometimes impulsive). Since the sample size is typically much smaller than the radiofrequency wavelength, the ($\Delta\mathbf{k}_j$) factors are not important and the signal is generated in all directions. However, the phase information may be retrieved in the time domain by scanning the phases of the various fields. Coming up with setups that will allow differentiation between various signals generated at different directions (phase matching) is a tough problem in multidimensional spectroscopies due to the many possible signals of different orders generated at very close directions.

In weak-field Raman techniques the signal decreases with the number of pulses since only a small fraction of molecules is affected by the application of each successive pulse. This is in marked contrast with strong-field NMR techniques where the entire ensemble is being manipulated, and there is no loss of intensity as the number of pulses is increased.

The classical visualization of spin dynamics was proposed by Felix Bloch right after the discovery of nuclear magnetic resonance; the spin's density matrix can be represented by a unit vector moving across the Bloch sphere. Using this picture, Erwin Hahn came up with the celebrated classical runners-in-a-race-track illustration of his spin echoes:[39] The race starts with the firing of the first pulse. After a time t_1, the second pulse reverses the momentum of each runner. When a time t_2 has passed after the second pulse, they all end up back in the original position. The position in the circular track represents the phase of each spin. Being in the same position means that all spins add up in phase, hence the large macroscopic polarization and the echo signal at $t_2 = t_1$. The complete formal equivalence of spins and optically driven two-level systems has been established by Feynmann, Vernon, and Hellwarth.[11] The runners' analogy thus applies to ordinary photon echoes as well.

A semiclassical picture can be developed as well for photon echoes in oscillator systems. The classical oscillator variables are simply their coordinates and momenta, and we need not allude to the Bloch sphere. The picture is based on wavepackets in phase space, representing the oscillator's density matrix.[40] The nonlinear response becomes classical either at high temperature or when nonlinearities are weak. Separate classical expansions (in powers of $\hbar$) have been developed in both limits[38,40] For Raman echoes, conducted with weak fields, the insightful runners-in-a-track picture does not apply. First the signal depends only on the small fraction of the molecules perturbed by the field but not on the entire ensemble. In addition, the second pulse does not reverse the momentum but merely gives the oscillator a kick (changing its momentum) in an amount that depends on the oscillator coordinates. This turns out to be sufficient for generating an echo. The common perception based on the NMR analogy that the echo is a strong-field phenomenon is incorrect. The echo has its roots in the weak-field regime. The strong-field ($\pi/2, \pi$) sequence will maximize the signal but is not essential for its origination.

In this Account we have demonstrated the capacity of multidimensional coherent Raman spectroscopies to provide a new window into molecular structure as well as intramolecular and intermolecular dynamical processes such as equilibrium fluctuations of local environments and vibrational energy transfer pathways. These techniques should be ideal for probing ultrafast processes including charge transfer and chemical reactions. Comparison of multidimensional NMR and vibrational spectroscopies will undoubtedly stimulate new experiments in both fields. The well-developed machinery of multiple pulse NMR may be adopted to probe specific vibrational motions and interactions. At the same time, the weak-field, low-temperature regime may offer new avenues for conducting NMR measurements and for their interpretation in terms of nonlinear susceptibilities. Sequences of multiquantum NMR coherences provide important structural tools since they are sensitive to geometry and coupling patterns. Vibrational Raman and infrared techniques have the potential to become as valuable.

S.M. gratefully acknowledges the support of a Guggenheim Fellowship and the Alexander von Humboldt Fellowship. The hospitality of Professor Ed Schlag at the Technical University of Munich is greatly appreciated. We gratefully acknowledge the support of the National Science Foundation and the United States Air Force Office of Scientific Research.

References

(1) Jimenez, R.; Fleming, G. R.; Kumar, P. V.; Maroncelli, M. Femtosecond solvation dynamics of water. *Nature* **1994**, *369*, 471.

(2) de Boeij, W. P.; Pshenichnikov, M. S.; Wiersma, D. A. System-Bath Correlation Function Probed by Conventional and Time-Gated Stimulated Photon Echo. *J. Phys. Chem.* **1996**, *100*, 11806.

(3) Rektor, K. D.; Kwok, A. S.; Ferrante, C.; Tokmakoff, A.; Rella, C. W.; Fayer, M. D. Vibrational Anharmonicity and Multilevel Vibrational Dephasing from Vibrational Echo Beats. *J. Chem. Phys.* **1997**, *106*, 10027.

(4) Narasimhan, L. R.; Littau, K. A.; Pack, D. W.; Eischner, Y. S. Bai; Fayer, M. D. Probing Organic Glasses at Low Temperature with Variable Time Scale Optical Dephasing Measurements. *Chem. Rev.* **1990**, *90*, 439.

(5) Jankowiak, R.; Small, G. J. Spectral Diffusion of Molecular Electronic Transitions in Amorphous Solids: Weak and Strong Two-Level-System Phonon Coupling. *Phys. Rev. B* **1993**, *47*, 14805.

(6) Jeckson, M.; Mantsch, H. The Use and Misuse of FTIR Spectroscopy in the Determination of Protein Structure. *Crit. Rev. Biochem. Mol. Biol.* **1995**, *30*, 95.

(7) Creighton, T. E. *Proteins: Structures and Molecular Properties*; 2nd ed.; W. H. Freeman: New York, 1993.

(8) Bratos, S.; Leicknam, J-Cl. Subpicosecond Transient Infrared Spectroscopy of Water: A Theoretical Discription. *J. Chem. Phys.* **1995**, *103*, 4887.

(9) Laenen, R.; Rauscher, C.; Laubereau, A. Dynamics of Local Substructures in Water Observed by Ultrafast Infrared Hole Burning. *Phys. Rev. Lett.* **1998**, *80*, 2622.

(10) Ernst, R. R.; Bodenhausen, G.; Wokaun, A. *Principles of Nuclear Magnetic Resonance in One and Two Dimensions*; Clarendon Press: Oxford, 1987. Sanders, J. K. M.; Hunter, B. H. *Modern NMR Spectroscopy*; Oxford: New York, 1993.

(11) Feynman, R. P.; Vernon, F. L.; Hellwarth, R. W. Geometrical Representation of the Schrodinger Equation for Solving Maser Problem. *J. Appl. Phys.* **1957**, *28*, 49.

(12) Leung, K. P.; Mossberg, T. W.; Hartman, S. R. Noble-Gas-Induced Collisional Broadening of the 6P1/2-6P3/2 Transitions of T1 Measured by Raman Echoes. *Phys. Rev. A* **1982**, *25*, 3097.

(13) Weiner, A. M.; Leird, D. E.; Weiderrecht, G. P.; Nelson, K. A. Femtosecond Pulse Sequences Used for Optical Manipulation of Molecular Motion. *Science* **1990**, *247*, 1317. Dugan, M.; Tull, J. X.; Warren, W. S. In *Ultrafast Phenomena* X; Barbara, P. F., Fujimoto, J. G., Knox, W. H., Zinth, W., Eds.; Springer: Berlin, 1996. Trembino, R.; DeLong, K. W.; Sweetser, J. N.; Krumbugel, M. A.; Richman, B. A.; Kane, D. J. Measuring Ultrafast Laser Pulses in the Time-Frequency Domain Using Frequency-Resolved Gating. *Rev. Sci. Instrum.* **1997**, *68*, 3277.

(14) Loring, R. F.; Mukamel, S. Selectivety in Coherent Raman Measurements of Vibrational Dephasing in Liquids. *J. Chem. Phys.* **1985**, *83*, 2116.

(15) Hellwarth, R. W. Third-Order Optical Susceptibilities of Liquids and Solids, *Prog. Quantum Electron.* **1977**, *5*, 2.

(16) Laubereau, A.; Kaiser, W. Vibrational Dynamics of Liquids and Solids Investigated by Picosecond Light Pulses. *Rev. Mod. Phys.* **1978**, *50*, 607. Zinth, W.; Leonhardt, R.; Holzapfel, H.; Kaiser, W. *IEEE J. Quantum Electron.* **1988**, *24*, 455.

(17) Inaba, R.; Okamoto, H.; Yoshihara, K.; Tasumi, M. *J. Phys. Chem.* **1993**, *97*, 7815. Libenberger, F.; Rauscher, C.; Purucker, H.-G.; Laubereau, A. Non-Exponential Dephasing of Molecular Vibrations in Liquids, Directly Observed by Magic' Femtosecond CARS. *J. Raman Spectrosc.* **1995**, *26*, 835. Joo, T.; Albrecht, A. C. Time-Resolved Coherent Stokes Raman Spectroscopy of Benzene. *J. Chem. Phys.* **1995**, *99*, 3244.

(18) Bruckner, V.; Bente, E. A. J. M.; Langelaar, J.; Bebelaar, D.; Van Voorst, J. D. W. Raman Echo on a Picosecond Timescale in Nitrogen Gas. *Opt. Commun.* **1984**, *51*, 49.

(19) Berg, M.; Bout, D. A. V. Ultrafast Raman Echo Measurements of Vibrational Dephasing and the Nature of Solvent-Solute Interactions. *Acc. Chem. Res.* **1997**, *30* 65.

(20) Tominaga, K.; Yoshihara, K. Fifth Order Response of Liquid CS_2, Observed by Ultrafast Nonresonant Six-Wave-Mixing. *Phys. Rev. Lett.* **1995**, *74*, 3061. Tominaga, K.; Yoshihara, K. Temporally Two-Dimensional Overtone Vibrational Dephasing Spectroscopy in Liquids. *Phys. Rev. A* **1997**, *55*, 831.

(21) Tanimura, Y.; Mukamel, S.; Two-Dimensional Femtosecond Vibrational Spectroscopy of Liquids. *J. Chem. Phys.* **1993**, *99*, 9496. Khidekel, V.; Mukamel, S.; High-Order Echoes in Vibrational Spectroscopy of Liquids. *Chem. Phys. Lett.* **1995**, *240*, 304.

(22) Steffen, T.; Fourkas, J. T.; Duppen, K. Time Resolved Four- and Six-Wave Mixing in Liquids. II. Experiments. *J. Chem. Phys.* **1997**, *106*, 3854.

(23) Tokmakoff, A.; Lang, M. J.; Larsen, D. S.; Fleming, G. R.; Chernyak, V.; Mukamel, S. Two-Dimensional Raman Spectroscopy of Vibrational Interactions in

Liquids. *Phys. Rev. Lett.* **1997**, *79*, 2702. Tokmakoff, A.; Fleming, G. R. Two-Dimensional Raman Spectroscopy of the Intermolecular Modes of Liquid CS_2. *J. Chem. Phys.* **1997**, *106*, 2569.

(24) Okumura, K.; Tanimura, Y. The (2n + 1)th-order Off-Resonant Spectroscopy from the (n + 1)th-order Anharmonicities of Molecular Vibrational Modes in the Condensed Phase. *J. Chem. Phys.* **1997**, *106*, 1687. Cho, M.; Okumura, K.; Tanimura, Y. Coherent Two-Dimensional Raman Scattering: Frequency-Domain Measurement of the Intra- and Intermolecular Vibrational Interactions. *J. Chem. Phys.* **1998**, *108*, 1326.

(25) Saito, S.; Ohmine, I. Off-Resonance Fifth Order Nonlinear Response of Water and CS_2 : Analysis Based on Normal Modes. *J. Chem. Phys.* **1998**, *108*, 240.

(26) Hamm, P.; Lim, M.; Hochstrasser, R. M. The Structure of the Amid I Band of Peptides Measured by Femtosecond Nonlinear IR Spectroscopy. *J. Phys. Chem. B.* **1998**, *102*, 6123.

(27) Mukamel, S. *Principles of Nonlinear Optical Spectroscopy*; Oxford University Press: New York, 1995.

(28) Yan, Y.-X.; Gamble, Jr., E. B.; Nelson, K. A. Impulsive Stimulated Scattering Important in Femtosecond Laser Pulse Interactions with Matter, and Spectroscopic Applications. *J. Chem. Phys.* **1985**, *83*, 5391. McMorrow, D.; Lotshaw, W. T.; Kenny-Wallace, G. A. Femtosecond Optical Kerr Studies on the Origin of the Nonlinear Responses in Simple Liquids. *IEEE Quantum Electron.* **1988**, *24*, 443. Nelson, K. A.; Ipper, E. P. Femtosecond Coherent Spectroscopy. *Adv. Chem. Phys.* **1989**, *75*, 1.

(29) Stratt, R. M. The Instantaneous Normal Modes of Liquids. *Acc. Chem. Res.* **1995**, *28*, 201. Keyes, T. Instantaneous Normal Mode Approach to Liquid State Dynamics. *J. Phys. Chem. A* **1997**, *101*, 2921.

(30) Leeson, D. T.; Wiersma, D. A. Real Time Observation of Low-Temperature Proteins Motions. *Phys. Rev. Lett.* **1995**, *74*, 2138.

(31) Chernyak, V.; Wang, N.; Mukamel, S. Four-Wave Mixing and Luminescence of Confined Excitons in Molecular Aggregates and Nanostructures. Many-Body Green Function Approach. *Phys. Rep.* **1995**, *263*, 213.

(32) Okumura, K.; Tanimura, Y. Sensitivity of Two-Dimensional Fifth-Order Raman Resonance to the Mechanism of Vibrational Mode-Mode Coupling in Liquid Molecules. *Chem. Phys. Lett.* **1997**, *278*, 175.

(33) Torii, H.; Tasumi, M. Model Calculations on the Amid-I Infrared Bands of Globular Proteins. *J. Chem. Phys.* **1992**, *96*, 3379.

(34) Stimson, M. J.; Ulness, D. J.; Albrecht, A. C. Frequency Resolved Interferometric Coherent Raman Spectroscopy with Incoherent Light: Raman Frequency Shifts, Dephasing Rate Constants, and Nonresonant Hyperpolarizabilities of Mixtures of Benzene in Hexane. *Chem. Phys.* **1997**, *222*, 17.

(35) Chernyak., V.; Piryatinski, A.; Mukamel, S. Complete Determination of Relaxation Parameters from Two-Dimensional Raman Spectroscopy. *Laser Chem.*, in press.

(36) Palese, S. P.; Buontempo, J. T.; Schilling, L.; Lotshaw, W. T.; Tanimura, Y.; Mukamel, S.; Miller, R. J. D. Femtosecond Two-Dimensional Raman Spectroscopy of Liquid Water. *J. Phys. Chem.* **1994**, *98*, 12466.

(37) Madden, P. A.; Tildesley, D. J. Interaction-Induced Contributions to Rayleigh and Allowed Raman Bands. A Simulation Study of CS_2. *Mol. Phys.* **1985**, *55*, 969. Geiger, L. C.; Ladanyi, B. M. Higher Order Interaction-Induced Effects on Rayleigh Light Scattering by Molecular Liquids. *J. Chem. Phys.* **1987**, *87*, 191.

(38) Mukamel, S.; Khidekel, V.; Chernyak, V. Classical Chaos and Fluctuation-Dissipation Relations for Nonlinear Response. *Phys. Rev. E.* **1996**, *53*, 1. Khidekel, V.; Chernyak, V.; Mukamel, S. Semiclassical Path-Integral Approach to Nonlinear Spectroscopy. In *Femtochemistry*; Chergui, M., Ed.; World Scientific: Singapore, 1996; p 507.

(39) Hahn, E. L. Spin Echo. *Phys. Rev.* **1950**, *80*, 583.

(40) Chernyak, V.; Mukamel, S. Multidimensional Femtosecond Spectroscopies of Vibrational Motions in Liquids: Semiclassical Expression. *J. Chem. Phys.* **1998**, *108*, 5812.

AR960206Y